



HAL
open science

**Synthesis of 1,3-butadiene from 1-butanol on a porous ceramic
[fe,cr]/gamma-al₂o₃(k,ce)/alpha-al(2)o(3)catalytic converter**

A. S. Fedotov, V. I. Uvarov, M. V. Tsodikov, I. I. Moiseev, Sébastien Paul, Svetlana Heyte Dyshlovenko, Pardis Simon, Maya Marinova, Franck Dumeignil

► **To cite this version:**

A. S. Fedotov, V. I. Uvarov, M. V. Tsodikov, I. I. Moiseev, Sébastien Paul, et al.. Synthesis of 1,3-butadiene from 1-butanol on a porous ceramic [fe,cr]/gamma-al₂o₃(k,ce)/alpha-al(2)o(3)catalytic converter. *Kinetics and Catalysis*, 2020, *Kinetics and Catalysis*, 61, pp.390-404. 10.1134/S002315842003009X . hal-04296579

HAL Id: hal-04296579

<https://hal.univ-lille.fr/hal-04296579>

Submitted on 20 Nov 2023

HAL is a multi-disciplinary open access archive for the deposit and dissemination of scientific research documents, whether they are published or not. The documents may come from teaching and research institutions in France or abroad, or from public or private research centers.

L'archive ouverte pluridisciplinaire **HAL**, est destinée au dépôt et à la diffusion de documents scientifiques de niveau recherche, publiés ou non, émanant des établissements d'enseignement et de recherche français ou étrangers, des laboratoires publics ou privés.

Synthesis of 1,3-Butadiene from 1-Butanol on a Porous Ceramic [Fe,Cr]/ γ -Al₂O₃(K,Ce)/ α -Al₂O₃ Catalytic Converter

A.S. Fedotov^{a, *}, V. I. Uvarov^b, M. V. Tsodikov^a, I. I. Moiseev^a, S. Paul^c, S. Heyte^c, P. Simon^c,
M. Marinova^d, and F. Dumeignil^c

^aTopchiev Institute of Petrochemical Synthesis, Russian Academy of Sciences, Moscow, 119991
Russia

^bMerzhanov Institute of Structural Macrokinetics and Materials Sciences, Russian Academy of
Sciences, Chernogolovka, Moscow oblast, 142432 Russia

^cUniversité de Lille, CNRS, Centrale Lille, ENSCL, Univ. Artois, UMR 8181-UCCS-Unité de
Catalyse et Chimie du Solide, Lille, F-59000 France

^dInstitut Chevreul, FR2638 CNRS, Bât. C6 Université Lille 1, Villeneuve d'Ascq, F-59655 France

*e-mail: alexey.fedotov@ips.ac.ru

Abstract – A two-stage method was developed for the synthesis of 1,3-butadiene by dehydration of 1-butanol to a mixture of butenes on γ -Al₂O₃ granules prepared by self-propagating high-temperature synthesis (SHS) followed by dehydrogenation of the butene fraction to 1,3-butadiene using a porous ceramic catalytic SHS converter [Fe,Cr]/ γ -Al₂O₃(K,Ce)/ α -Al₂O₃. The dehydration of 1-butanol to the butene mixture proceeded almost completely at ~100% selectivity on γ -Al₂O₃ granules obtained by SHS at 300 °C, which is 50 degrees lower than on industrial gamma-alumina granules. The use of an original hybrid catalytic membrane reactor (HCMR) with selective removal of hydrogen from the reaction zone led to a ~1.3-fold increase in the yield of 1,3-butadiene at ultrapure hydrogen extraction of up to 16 mol % of the total amount of the hydrogen product. The catalytic activity of the system did not decrease after 20 h of experiment, in contrast to its activity in the industrial process, where catalyst regeneration is performed every 8–15 min.

Keywords: heterogeneous catalysis, porous ceramic catalytic converter, self-propagating high-temperature synthesis, catalytic membrane reactor, dehydration of biobutanol, dehydrogenation of butenes, monomer synthesis, 1,3-butadiene synthesis, release of ultrapure hydrogen

Abbreviations: GLC, gas-liquid chromatography; GC-MS, gas chromatography-mass spectrometry; FID, flame ionization detector; HCMR, hybrid catalytic membrane reactor; SHS, self-propagating high-temperature synthesis; SEM-EDX, scanning electron microscopy with energy dispersive X-ray spectroscopy; TGA, thermogravimetric analysis; TPR_{reduction-H₂}, thermally programmed reduction with hydrogen; TEM, transmission electron microscopy; XPS, X-ray photoelectron spectroscopy.

INTRODUCTION

Since the early 20th century when S.V. Lebedev's work was published, alcohols have been the raw materials for the industrial production of 1,3-butadiene, which is one of the main monomers for the synthesis of artificial rubbers [1]. Today the general trend is additionally a transition to renewable resources. The synthesis of 1,3-butadiene was the subject of many studies [2, 3]. Despite the rich history of the development of methods for its synthesis, the selectivity of transformations still remains a challenge. As the reaction is endothermic, it is necessary to maintain

high temperature in the reactor, which promotes side reactions, leading to quick coking of catalysts [4]. Therefore, the world's leading scientific schools are searching for alternative approaches to the development of environmentally friendly and effective processes for the production of 1,3-butadiene [5].

1,3-Butadiene is the most important monomer with global production of over 12 million t/year [6], which is mainly used for the synthesis of butadiene-styrene (28%) and polybutadiene (26%) rubbers widely used in tire industry. Currently, 1,3-butadiene is obtained by three main methods [7]: steam cracking of paraffin hydrocarbons, where butadiene is a by-product of ethylene production (more than 95% of world production); catalytic dehydrogenation of butane-butene fractions (less than 2%); and oxidative and vapor-oxidative dehydrogenation of butenes (the rest). Importantly, the monomer production includes numerous stages, such as oil refining, organic synthesis, separation of hydrocarbon mixtures, etc. Thus, all the proposed methods for butadiene synthesis are capital intensive, and the use of fossil fuels as raw materials increases the environmental load on the production sites [8].

From the viewpoint of rational nature management, the monomer synthesis should utilize the by-products of alcohol fermentation, for example, 1-butanol [9], by its dehydration to the butene fraction followed by dehydrogenation to 1,3-butadiene.

Butanol is now considered as a high-octane additive to gasoline fuel, whose technical characteristics are significantly higher than those of ethanol. For this reason, several large companies decided to develop processes aimed at increasing butanol production [10–12]. In addition, 1-butanol can serve as a raw material for biofuel production [13, 14].

Butanol, like ethanol, can be synthesized by processing sugar or starch of agricultural crops (first-generation biobutanol) and cellulose (second-generation biobutanol). As the biobutanol market has already reached 5 billion L/year [15], it is potentially of interest for obtaining additional quantities of butadiene at decentralized low-tonnage enterprises, which may be important for regions remote from the sites of large petrochemical plants. For example, in 2016, the production of high-purity bio-1-butanol was commercialized by Green Biologics (Great Britain) at its new industrial facilities in Little Falls (Minnesota, United States) [16].

It is also important that recently, the scientific basis for breakthrough technologies for direct production of 1-butanol from ethanol has been developed, by performing the reaction of EtOH in a supercritical state with a record yield of 1-butanol of ~60% at 85–90% selectivity, while the yield of 1-butanol in fermentation processes does not exceed 10% [12, 17, 18]. Therefore, the use of 1-butanol for the production of synthetic rubbers may become another important stage in the development of environmentally friendly chemical industries based on renewable raw materials.

One promising way to solve this problem is the use of hybrid membrane catalytic technology. In this technology, the total energy of the process is reduced due to a combination of stages in one device: the reaction stage proceeding in the channels of a porous catalytic converter obtained by self-propagating high-temperature synthesis (SHS) and the hydrogen separation stage on a palladium-containing membrane integrated into the cavity of the converter. Due to this, the dimensions of the unit are significantly reduced, the hardware design is significantly simplified, and high-purity products can be obtained with higher yields at the outlet of the reactor than in a conventional reactor with a stationary bed of bulk catalyst. The efficiency of this approach was confirmed by previous studies on the production of ultrapure hydrogen in carbon-dioxide, steam, and mixed reforming of methane, ethanol, fermentation products, and dimethyl ether [19–21].

1. EXPERIMENTAL

1.1 Synthesis of Porous Catalytic Materials for the Production of 1,3-Butadiene from 1-Butanol

1.1.1 SHS of γ -Al₂O₃ granules. To perform SHS of the butene fraction from 1-butanol, γ -Al₂O₃ granules were obtained. The fraction was synthesized from a gel of a pseudoboehmite AlOOH structure using single-action compacting at a pressure of 30–90 MPa followed by sintering at 750 °C in air for 1 h. The diameter of the open pores of the synthesized sample determined with a mercury porosimeter and by the bubble method was ~1–3 μ m. The porosity of the samples measured by hydrostatic weighing was ~40%.

1.1.2. Preparation of a tubular porous ceramic support based on α -Al₂O₃ by SHS. The raw material for the preparation of a tubular porous ceramic support was α -Al₂O₃ powder of a large fraction of “Electrocorundum white” with a particle size of 100 μ m (Litprom).

To increase the mechanical strength of the support and its resistance to high temperature, powder additives of eutectic composition were introduced in the initial α -Al₂O₃ powder: magnesium oxide (GOST (State Standard) 4526-75, Krasnyi Khimik (Red Chemist) plant) and silicon carbide in a ratio of 90 wt % α -Al₂O₃, 3 wt % MgO, and 7 wt % SiC. During the SHS, these compounds form active SiO₂, which binds α -Al₂O₃ particles with one another due to their transformation into mullites, indialite (Mg₂Al₄Si₅O₁₈), and spinel (MgAl₂O₄).

The powders were mixed in a ball mill for 1 h. The finished mixture was subjected to single-action compacting at a pressure of 30–90 MPa, sintered at 1300–1450 °C in air for 1 h, and cooled to room temperature for 2 h.

At powder sintering temperatures in the range 1300–1450 °C, a liquid phase of eutectic composition forms, which contains magnesium oxide and silicon carbide in the form of clinoenstatite, which wets Al₂O₃ particles, forming a strong porous support frame. For easy recording of the catalyst composition, the tubular ceramic support is denoted below as α -Al₂O₃ without mentioning the additives.

The porous ceramic support is a tube with a dead end to provide forced diffusion of gases through the cylinder’s working surface from outer to inner wall, and the other end of the tube has a hold-down nut for hermetically joining the tubular support with the reactor through a graphite gasket (Fig. 1). The tube channel is intended for introducing a hydrogen-selective palladium-containing membrane and removing the unchanged substrates and unfiltered reaction products from the reactor [19].

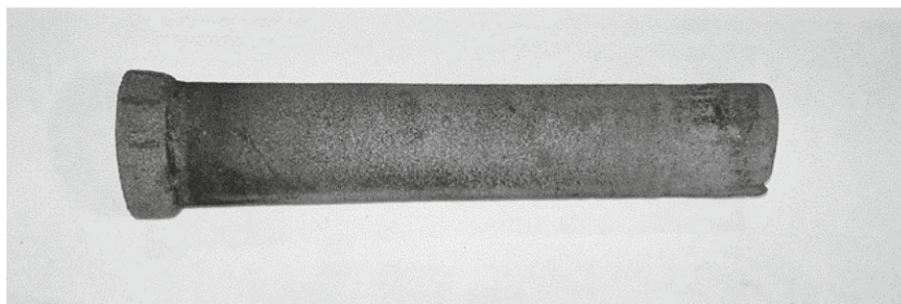


Fig. 1. Tubular porous ceramic support consisting of α -Al₂O₃.

The geometrical dimensions of the tubular support were: total length 137 mm, working area length 120 mm, outer diameter of the tube 25 mm, and wall thickness 7 mm.

The open pore size of the tubular porous ceramic support was evaluated according to the capillary displacement model based on the Laplace formula for the cylindrical pore model using

a mercury porometer and by the bubble method [22]. The open pore diameter of the support was 1–3 μm . The porosity measured by hydrostatic weighing was more than 50%.

1.2 Modification of the Tubular Porous Ceramic Support with Iron-, Chromium-, and Manganese-Containing Mono- and Bimetal Catalysts

To impart the catalytic properties necessary for dehydrogenation of butenes to the tubular porous ceramic support, it was modified with various active components.

To determine the optimum composition of the catalyst for butene dehydrogenation, model granular catalysts were used in a flow reactor at the first stage of the study: $\text{Mn}/\gamma\text{-Al}_2\text{O}_3(\text{K,Ce})$; $\text{Fe,Mn}/\gamma\text{-Al}_2\text{O}_3(\text{K,Ce})$ (separate deposition of Fe and Mn); $[\text{Fe} + \text{Mn}]/\gamma\text{-Al}_2\text{O}_3(\text{K,Ce})$ (combined deposition of Fe and Mn); and $[\text{Fe} + \text{Mn}]/\gamma\text{-Al}_2\text{O}_3(\text{K,Ce})$ (separate deposition of Fe and Cr).

The support was $\gamma\text{-Al}_2\text{O}_3$ (sphere 0.8 mm, $S_{\text{sp}} = 205 \text{ m}^2/\text{g}$) (SKTB Katalizator, Novosibirsk). In all the cases, the initial $\gamma\text{-Al}_2\text{O}_3$ was first dried in a vacuum

drier at 100 $^\circ\text{C}$ for 3 h, and then modifying additives were introduced by separate impregnation of alumina with aqueous solutions of potassium carbonate (K_2CO_3) and cerium nitrate $[\text{Ce}(\text{NO}_3)_3 \cdot 6\text{H}_2\text{O}]$. These components were applied to a porous ceramic support to suppress side reactions [23]. After the impregnation, the thus modified support was dried in a flow of warm air at 40 $^\circ\text{C}$, then in a drier at 120 $^\circ\text{C}$ for 3 h and calcinated in a muffle furnace at 500 $^\circ\text{C}$ for 4 h. Then the precursors of active components were applied to it in layers from aqueous and organic solutions.

$\text{Mn}/\gamma\text{-Al}_2\text{O}_3(\text{K,Ce})$. Manganese was deposited by impregnating modified alumina with an aqueous solution of manganese acetate $\text{Mn}(\text{OAc})_2 \cdot 4\text{H}_2\text{O}$.

$\text{Fe,Mn}/\gamma\text{-Al}_2\text{O}_3(\text{K,Ce})$. At first, iron was applied from aqueous iron nitrate $\text{Fe}(\text{NO}_3)_3 \cdot 9\text{H}_2\text{O}$; then, after drying and thermal shock at 500 $^\circ\text{C}$ for 30 min, manganese was applied from aqueous manganese acetate.

$[\text{Fe}+\text{Mn}]/\gamma\text{-Al}_2\text{O}_3(\text{K,Ce})$. Iron and manganese were simultaneously deposited from an aqueous solution containing iron nitrate and manganese acetate, then dried and calcinated.

$[\text{Fe,Cr}]/\gamma\text{-Al}_2\text{O}_3(\text{K,Ce})$. Iron and chromium were deposited by separate impregnation with a toluene or mixed toluene–benzene solution containing iron and chromium acetyl acetonates $\text{Fe}(\text{acac})_3$ and $\text{Cr}(\text{acac})_3$.

The final two-stage calcination of all the samples was performed in a muffle furnace at a temperature rise rate of 10 deg/min, allowing them to stand at 500 $^\circ\text{C}$ for 3 h and at 800 $^\circ\text{C}$ for 2 h.

The composition of the prepared catalysts is given in Table 1.

Table 1. Composition of the model catalysts of dehydrogenation.

Catalyst	Composition (oxides)	Content, g	Content, wt %
$\text{Mn}/\gamma\text{-Al}_2\text{O}_3(\text{K,Ce})$	$\gamma\text{-Al}_2\text{O}_3$	18.80	87.69
	K_2O	0.32	1.48
	CeO_2	0.21	0.97
	Mn_2O_3	2.11	9.86
$\text{Fe,Mn}/\gamma\text{-Al}_2\text{O}_3(\text{K,Ce})$, separate	$\gamma\text{-Al}_2\text{O}_3$	18.84	88.36

deposition of Fe and Mn	K ₂ O	0.28	1.33
	CeO ₂	0.21	0.96
	Fe ₂ O ₃	1.00	4.70
	Mn ₂ O ₃	0.99	4.65
[Fe+Mn]/ γ -Al ₂ O ₃ (K,Ce), co-deposition of Fe and Mn	γ -Al ₂ O ₃	18.16	85.52
	K ₂ O	0.40	1.90
	CeO ₂	0.18	0.85
	(Fe,Mn) ₂ O ₃	2.49	11.73
[Fe,Cr]/ γ -Al ₂ O ₃ (K,Ce), separate deposition of Fe and Cr	γ -Al ₂ O ₃	17.80	90.30
	K ₂ O	0.30	1.50
	CeO ₂	0.16	0.80
	(Fe,Cr) ₂ O ₃	1.46	7.40

The tubular porous ceramic supports with a preliminary deposited intermediate layer of γ -Al₂O₃, formed in order to increase the pore surface, were modified in a similar way, by molecular layering of a colloidal solution of the precursor of the active component on the pore surface. For this, a colloidal solution of a sol consisting of H₂O (0.03 mol %), 1.5 M

Al(OPri)₃, and acetylacetone (1.5 mol) in toluene was applied by injecting it through the pores of the sample at the first stage. After the sol was applied, the modified porous ceramic support was dried in a flow of air in a drier at 120 °C for 1 h, and then heat treatment was performed in a thermal shock mode at 500 °C for 30 min. The amount of deposited γ -Al₂O₃ was evaluated from the increase in the mass of the sample. The impregnation step was repeated four times until the mass gain reached 4–5 wt %. Then, K₂O and CeO₂ were applied by separately impregnating the converter with aqueous potassium carbonate and cerium nitrate.

The active Fe- and Cr-containing components were separately deposited on the modified support from the toluene solutions of the corresponding acetyl acetonate complexes containing 7.2 wt % Fe(acac)₃ and 7.4 wt % Cr(acac)₃. To form Fe(III) and Cr(III) oxides, the impregnated sample was calcinated in a muffle furnace in an air flow at 500 °C for 2 h, 600 °C for 2 h, and 800 °C for 1 h. The amount of the deposited components was determined by weight gain of the sample after all stages of heat treatment.

The contents of the components of the [Fe,Cr]/ γ -Al₂O₃(K,Ce)/ α -Al₂O₃ catalytic converters of dehydrogenation of the butene fraction are listed below:

K ₂ O	CeO ₂	(Fe,Cr) ₂ O ₃ (1:1)	γ -Al ₂ O ₃	α -Al ₂ O ₃
0.12	0.04	0.50	4.53	94.81

The sample of the porous ceramic support prepared from α -Al₂O₃ and modified with the catalytically active components is called below a “converter.” The catalytic experiments used both the whole converter and the granules obtained by mechanical crushing (granular converter).

The butene fraction diluted with argon and obtained in reactor 1 (23) was separated from the liquid phase containing a small amount of unchanged 1-butanol and water formed during the dehydration in a water-cooled separator (34). The dried argon-butene mixture, preliminarily mixed with water to reduce the partial pressure of butenes, went to the dehydrogenation stage along a network of pipelines through T-joints (37 and 10) into reactor 2 (24). Water was supplied from a liquid doser (7) through a mixing T-joint (11), and the mixture was heated in an evaporator (16). Butenes were dehydrogenated to 1,3-butadiene on the granules of model catalysts and on the synthesized tube or granular converter in a hybrid membrane-catalytic reactor (HMCR) (Fig. 3) the same to the one described in [19]. The reactor was made of steel 20X23X18. The conditions of dehydrogenation corresponded to the industrial conditions (except the mass of the catalyst charge): mgr.cat. = 14.75 g; excess H₂O: ×0, ×10, ×20, ×30; space velocity of the vapor-gas mixture $Q_{v-g} = 597 \text{ h}^{-1}$; $T = 637 \text{ }^\circ\text{C}$; and $P_{\text{tot}} = 1 \text{ atm}$.

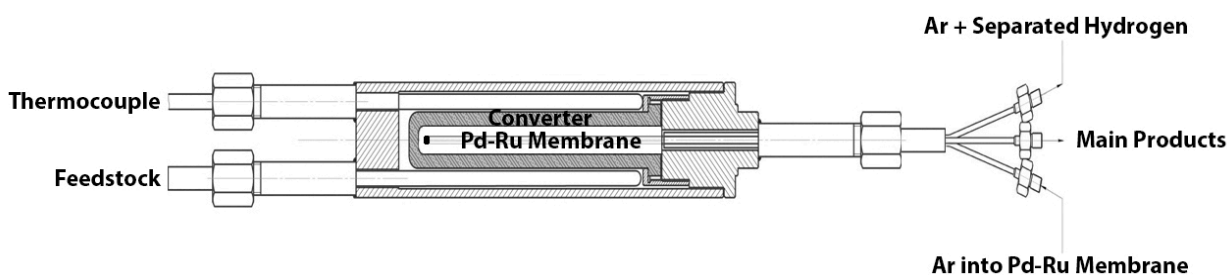


Fig. 3. Hybrid catalytic membrane reactor for dehydrogenation of the butylene fraction with an installed tubular $[\text{Fe,Cr}]/\gamma\text{-Al}_2\text{O}_3(\text{K,Ce})/\alpha\text{-Al}_2\text{O}_3$ catalytic converter.

The gas mixture obtained at the outlet of reactor 2 (24) and containing the desired 1,3-butadiene product was separated from the liquid phase in a water-cooled separator (27) and forwarded to the instrument for online gas chromatographic analysis (43).

To evaluate the contribution of the material of an empty reactor to dehydrogenation, a comparative idle experiment was performed in it under the same conditions as on the catalytic converters.

1.4 Method for Analysis of Reaction Products

The contents of hydrogen, carbon oxides, and methane in the reaction products were determined online by gas chromatography on a Crystallux-4000M chromatograph (Meta-chrom, Russia) using a thermal conductivity detector; the carrier gas was high-purity argon with a flow rate of 10 mL/min; the adsorption packed column was 1 m × 3 mm. The column packing was activated carbon SKT; the particle size was 0.2–0.3 mm. The temperature of the column, detector, and evaporator was 120 °C. The gas concentrations were found from the calibration curves using specialized NetChrom v2.1 software. The low concentrations of carbon monoxide were determined using a calibrated RI-550A IR spectrometer (Riken Keiki, Japan).

The C₁–C₄ hydrocarbon gases were identified on a Crystallux-4000M chromatograph using a flame ionization detector (FID) and helium as a carrier gas. The following gas flow rates were determined: helium 30 mL/min; hydrogen 35 mL/min; and air 300 mL/min. An HP-PLOT/Al₂O₃ chromatographic column was used (Agilent Technologies, United States; 50 m × 0.32 mm, film thickness 8.0 μm). The temperature was 120 °C (column), 230 °C (detector), and 250 °C (evaporator). The product concentration was determined from the calibration curves using specialized NetChrom v2.1 software.

The liquid organic products of the reaction in the organic phase were identified by GLC on a Varian 3600 chromatograph (Varian Chromatography System, United States), FID, Chromatec SE-30 capillary column, 25 m × 0.25 mm, Df = 0.33 μm. The temperature conditions: 50 °C (5 min), 10 °C/min, 280 °C, T_{inj} = 250 °C, P_{inj} = 1 bar, 1/200 flow division, helium carrier gas. The internal standards: trifluoromethyl-benzene for the alkane-olefin fraction and n-octane for the alcohol mixture. The residual content of organic products in the aqueous phase was found from the ratio of integrated signals by absolute calibration using GC-MS.

1.5 Structural Analysis Method

The carbon content in the spent catalyst was determined by thermogravimetric analysis (TGA) on an SDT Q600 instrument (TA Instruments, United States) (TG analyzer and differential scanning calorimeter) in an air flow. The conditions of TGA: sample 26.2 g, heating rate 10 °C/min, air flow rate 100 mL/min, temperature range 25–700 °C.

The thermally programmed reduction with hydrogen (TPR-H₂) of the initial [Fe,Cr]/γ-Al₂O₃(K,Ce)/

α-Al₂O₃ converter was performed on an AutoChem II 2920 Chemisorption Analyzer (Micromeritics, United States). Experimental conditions: sample 0.2 mg, composition of the gas mixture 5% H₂+Ar, gas flow rate 50 mL/min, heating rate 10 °C/min, temperature range 25–1000 °C.

The photomicrographs of the converters and the distribution of elements on the surface were obtained by scanning electron microscopy with energy dispersive X-ray spectroscopic analysis (SEM-EDX) on an S-3600N instrument (Hitachi, Japan) with the following operating parameters: accelerating voltage 20.0 kV, 200-fold resolution.

The structure of the material of the catalytic converter and the distribution of elements on its surface were studied by transmission electron microscopy on a TEM TITAN Themis 300 instrument (FEI, United States).

The surface analysis was performed by X-ray photoelectron spectroscopy (XPS) on an Axis Ultra DLD instrument (Kratos Analytical, Great Britain) with monochromatic AlK_α X-radiation (15 kV, 15 mA, 1486.6 eV). All the spectra were calibrated in energy using the position of the C1s peak corresponding to the C–C and C–H bonds at 284.8 eV.

1.6. Calculation Procedure

The process parameters were calculated by Eqs. (1)–(6).

1-butanol conversion:

$$X_{\text{BuOH}} = \frac{n_{\text{butene}}}{n_{\text{BuOH}}} \cdot 100\% \quad (1)$$

Butene conversion:

$$X_{\text{butylene}} = \frac{n_{\text{converted butene}}}{n_{\text{initial butene}}} \cdot 100\% \quad (2)$$

Yield of 1,3-butadiene:

$$x_{1,3\text{-butadiene}} = \frac{n_{1,3\text{-butadiene}}}{n_{\text{butene initial}}} \cdot 100\% \quad (3)$$

Selectivity to 1,3-butadiene (based on converted 1-butanol):

$$S_{\text{BuOH}} = \frac{n_{1,3\text{-butadiene}}}{n_{\text{BuOH}}} \cdot 100\% \quad (4)$$

Productivity of 1,3-butadiene in L/(h·g_{act.comp.}) ($V_{1,3\text{-butadiene}}$ – monomer stream in L/h; $m_{\text{act.comp.}}$ – mass of impregnated catalyst in g.):

$$\rho_{1,3\text{-butadiene}} = \frac{V_{1,3\text{-butadiene}}}{m_{\text{act.comp.}}} \cdot 100\% \quad (5)$$

Degree of hydrogen extraction in mol.% on the palladium-containing membrane:

$$N_{\text{hydrogen}} = \frac{n_{\text{hydrogen extracted}}}{n_{\text{hydrogen total}}} \cdot 100\% \quad (6)$$

In Eqs (1)-(6):

n_{butenes} is the molar flow of butene products formed during the dehydration of 1-butanol, mmol/h;

n_{BuOH} is the molar flow of 1-butanol fed for dehydration, mmol/h;

$n_{\text{transf. butenes}}$ is the molar flow of butenes transformed during the dehydrogenation, mmol/h;

$n_{\text{fed butenes}}$ is the molar flow of butenes fed for dehydrogenation, mmol/h;

$n_{1,3\text{-butadiene}}$ is the molar flow of 1,3-butadiene formed during the dehydrogenation of butenes, mmol/h;

$n_{\text{extr. hydr.}}$ is the molar flow of hydrogen extracted on the palladium-containing membrane, mmol/h;

$n_{\text{total hydr.}}$ is the total molar flow of hydrogen including the extracted and nonextracted hydrogen, mmol/h;

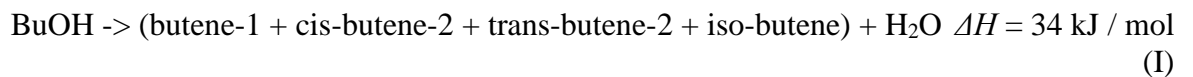
$V_{1,3\text{-butadiene}}$ is the molar flow of 1,3-butadiene that formed during the dehydrogenation of butenes, L/h;

$m_{\text{act. comp.}}$ is the mass of the catalytically active component deposited on the porous surface of the converter, g.

4. RESULTS AND DISCUSSION

4.1 Synthesis of 1,3-Butadiene

Stage 1: Dehydration of 1-butanol; synthesis of the butene fraction. The catalytic dehydration of 1-butanol leads to the formation of four butene isomers:



Our experiments on industrial $\gamma\text{-Al}_2\text{O}_3$ granules and contained predominantly butene-1 (Table 2). The concentration of butene-1 depends on the process conditions and the type of the catalyst used. In the presence of commercially available $\gamma\text{-Al}_2\text{O}_3$ granules, the concentration was 97% at 300 °C. On the sample prepared by SHS, the selectivity for butene-1 was slightly lower, 83% at the same temperature, which is probably due to the lower acidity of the active sites of the synthesized material [24]. In addition to butene-1, the butene fraction contained the cis-, trans-, and branched isomers; when the temperature increased to 350 °C, the proportion of the latter increased to 24% for commercially available granules and to 63% for the synthesized sample. This change in the isomer ratio does not affect further dehydrogenation because all the three isomers are converted into 1,3-butadiene [25]. The by-products contained traces of hydrocarbons from hydrogenation, cracking, and isomerization such as ethylene, propylene, butane, and isobutane, as well as hydrogen. The total concentration of by-products did not exceed 0.12% (Table 2). Importantly, dibutyl ether was not detected in the products. This evidently indicates that dehydration of 1-butanol mainly occurred at various active centers remote from one another, which excludes the interaction of adsorbed butanol molecules with one another. Another reason for the

almost complete absence of esterification products is the low partial pressure of the substrate [24, 26, 27]. The activity of the studied catalysts did not decrease throughout the experiment (30 h).

At 300 °C, the conversion of 1-butanol was ~66% on industrial γ -Al₂O₃ granules and close to 100% on the γ -Al₂O₃ sample prepared by SHS (Table 2). It was found that almost complete conversion of 1-butanol on industrial γ -Al₂O₃ granules could be achieved only at 350 °C.

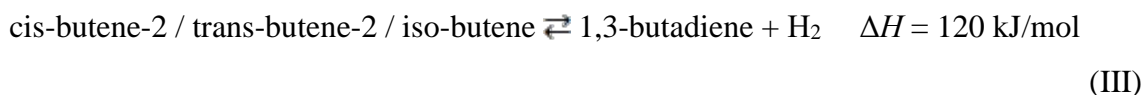
It can be assumed that the increase in the conversion of 1-butanol at 300 °C on γ -Al₂O₃ granules synthesized by SHS is due to the improved mass and heat transfer of the substrate in the synthesized porous material compared to those of industrial granules.

After the separation of the formed water and trace amounts of unchanged 1-butanol in the separator, the reaction products were forwarded, without preliminary gas purification and fractionation, to the second reactor for dehydrogenation of the butene fraction into 1,3-butadiene.

Table 2. Composition of the products of dehydration of 1-butanol at 300 and 350 °C on industrial γ -Al₂O₃ granules and on granulated γ -Al₂O₃ synthesized by SHS.

Component of product mixture	Industrial γ -Al ₂ O ₃ granules		Granulated γ -Al ₂ O ₃ synthesized by SHS	
	300 °C, $X_{\text{BuOH}} = 66\%$	350 °C, $X_{\text{BuOH}} = 100\%$	300 °C, $X_{\text{BuOH}} = 100\%$	350 °C, $X_{\text{BuOH}} = 100\%$
	C, vol %	C, vol %	C, vol %	C, vol %
Ethylene	0	0	0	0.03
Propylene	0	0	0	0.03
Butene-1	96.75	76.20	83.26	36.35
<i>iso</i> -Butene	0.11	0.12	0.11	0.21
<i>trans</i> -Butene-2	0.83	6.60	3.95	29.67
<i>cis</i> -Butene-2	2.31	17.08	12.57	33.59
1,3-Butadiene	0	0	0	0
Hydrogen	0	0	0.03	0.06
<i>n</i> -, <i>iso</i> -Butane	0	0	0.08	0.06

Stage 2: Dehydrogenation of the butene fraction; synthesis of 1,3-butadiene. The catalytic dehydrogenation of the butene fraction to 1,3-butadiene is an endo- thermal process, which proceeds in accordance with the following equations [25]:



The results of the idle experiment in a catalyst-free stainless steel flow reactor showed that the side processes of the destruction of the carbon skeleton of the initial butene fraction were dominant and formed a large amount of coke.

In order to find the optimum conditions, the process was performed both in a flow mode (contactor) using a conventional reactor with a bulk layer of granular catalyst and in a membrane mode (extractor) using an original membrane-catalytic hybrid reactor with an integrated hydrogen-selective palladium-containing membrane [19].

To determine the optimum process conditions and the composition of the butene dehydrogenation catalyst at the first stage of the study in a flow reactor, the process was studied

in the presence of granular model catalysts: α -Al₂O₃; Mn/ γ -Al₂O₃(K,Ce); [Fe,Mn]/ γ -Al₂O₃(K,Ce) (separate deposition); [Fe + Mn]/ γ -Al₂O₃(K,Ce) (co-deposition); [Fe,Cr]/ γ -Al₂O₃(K,Ce) (separate deposition).

At first, comparative experiments were performed on a tubular support based on α -Al₂O₃ and synthesized by SHS and on manganese-containing model catalysts. As a result, it was found that 20-fold dilution of the reagents with water was optimum and led to an approximately ninefold increase in the yield of 1,3-butadiene compared with its yield in experiments at lower dilution (experiments 5–20, Table 3). Twenty-fold dilution also decreased the concentration of cracking and pyrolysis products approximately three-fold. Thirty-fold dilution of reagents with water did not lead to a significant increase in the yield of 1,3-butadiene, which is probably due to the competing adsorption of water molecules at the active sites of the catalyst (experiments 3, 4; 7, 8; 11, 12; 15, 16; 19, 20; Table 3).

An experiment was performed, using the obtained optimum conditions for dilution of the butene fraction with water vapor, on the preparation of 1,3-butadiene on the synthesized [Fe,Cr]/ γ -Al₂O₃(K,Ce) model catalyst containing active components similar to those of the industrial catalyst for dehydrogenation of the butane–butene fraction (experiment 26, Table 4).

In view of its higher stability compared to manganese-containing catalysts in the process under study, the iron-chromium-containing system was chosen for the synthesis of the [Fe,Cr]/(K,Ce) γ -Al₂O₃/ α -Al₂O₃ converter. According to experiment 26 (Table 4), the yield of 1,3-butadiene on the synthesized integral converter was 18.8% at ~19.2% selectivity based on the initial 1-butanol.

The use of integral [Fe,Cr]/ γ -Al₂O₃(K,Ce)/ α -Al₂O₃ converter in the mode of hydrogen extraction from the reaction zone on a palladium-containing membrane allows us to increase the 1,3-butadiene yield and productivity ~1.3-fold (experiment 27, Table 3).

An increase in the yield of 1,3-butadiene in the case of using the integral converter may indicate an increase in the probability of the contact of substrate molecules with the active surface during the reaction in the forced diffusion mode in a limited space of the catalytic channels of the converter.

It was shown that dehydrogenation of butenes on the [Fe,Cr]/ γ -Al₂O₃(K,Ce)/ α -Al₂O₃ converter in the mode of ultrapure hydrogen extraction from the reaction zone on a palladium-containing membrane generally promotes the process (Table 4).

In addition to the main dehydrogenation reaction, side cracking reactions occur at temperatures above 600 °C, forming mainly propylene, ethylene, and methane (Table 4).

Thus, the use of the developed two-stage scheme for conversion of 1-butanol into 1,3-butadiene allows us to obtain a valuable monomer with high efficiency from biomass fermentation products with simultaneous release of ultrapure hydrogen, which is a useful raw material for organic synthesis and environmentally safe fuel for hydrogen internal combustion engines and fuel cells.

Importantly, the process occurring in the catalytic channels of the converter significantly decreases the intensity of coke formation. When the reaction is performed on the granular converter, the catalytic activity of the system decreases already after 20–30 min work. The palladium-containing hydrogen-selective HMCR membrane used in the dehydrogenation of the butene fraction with integral converter remains clean (Fig. 4a), but is carbonized after the experiment on the same composition, which lasts for the same period of time (Fig. 4b).

The significantly higher resistance of the integral converter to surface carbonization was confirmed by the thermogravimetric and structural analysis data.

Table 3. Dehydrogenation of the butane fraction*

Experiment no.	Catalyst composition	x-Fold dilution with water	Yield of 1,3-butadiene, %	Selectivity of formation of 1,3-butadiene**, %	1,3-Butadiene output, L h ⁻¹ g _{act.comp.} ⁻¹
1	Reactor without catalyst: idle experiment	0	2.7	3.6	–
2		10	7.3	6.8	–
3		20	6.4	6.2	–
4		30	5.0	4.8	–
5	Tubular α -Al ₂ O ₃ support	0	3.8	5.0	–
6		10	8.5	9.1	–
7		20	7.3	7.7	–
8		30	6.1	6.1	–
Modified industrial α -Al ₂ O ₃ granules in a mode without hydrogen extraction (contactor)					
9	[Fe+Mn]/ γ -Al ₂ O ₃ (K,Ce)	0	1.4	2.0	0.2
10		10	9.5	10.4	1.1
11		20	8.8	9.6	1.1
12		30	8.7	9.2	1.0
13	[Fe,Mn]/ γ -Al ₂ O ₃ (K,Ce)	0	2.4	3.5	0.3
14		10	10.0	11.5	1.2
15		20	11.8	13.7	1.5
16		30	12.4	13.9	1.5
17	Mn/ γ -Al ₂ O ₃ (K,Ce)	0	1.3	1.8	0.1
18		10	8.5	8.8	0.9
19		20	9.2	10.1	1.0
20		30	10.4	11.6	1.1
21	[Fe,Cr]/ γ -Al ₂ O ₃ (K,Ce)	20	9.0	8.3	1.1
Granulated modified converter in a mode without hydrogen extraction (contactor)					
22	[Fe,Cr]/ γ -Al ₂ O ₃ (K,Ce)/ α -Al ₂ O ₃	20	4.2	9.2	1.6
Granulated modified converter in a mode with hydrogen extraction (extractor)					
23	[Fe,Cr]/ γ -Al ₂ O ₃ (K,Ce)/ α -Al ₂ O ₃	20	7.8	11.7	2.0
Integral modified converter in a mode without hydrogen extraction (contactor)					
24	[Fe,Cr]/(K,Ce) γ -Al ₂ O ₃ / α -Al ₂ O ₃	0	1.7	2.0	0.2
25		10	13.1	14.6	1.6
26		20	18.8	19.2	2.3
Integral modified converter in a mode with hydrogen extraction (extractor)					
27	[Fe,Cr]/(K,Ce) γ -Al ₂ O ₃ / α -Al ₂ O ₃	20	23.2	23.7	2.9

* Process conditions: $n_{\text{butenes}} = 66.90$ mmol/h, $T = 637$ °C, $P_{\text{tot}} = 1$ atm.

** Selectivity of formation of 1,3-butadiene based on the initial 1-butanol. The dash means that it was impossible to calculate the output per gram of active component in the uncharged reactor and on alumina granules because of the absence of the active component.

Table 4. Composition and mole flows (mmol/h) of the products of butene dehydration on the granulated and integral [Fe,Cr]/ γ -Al₂O₃(K,Ce)/ α -Al₂O₃ converters in a mode without extraction and with extraction of ultrapure hydrogen from the reaction zone on a Pd–Ru membrane.

Convectormode	Conversion on the initial butene fraction, %	Reaction products**, mmol/h								
		butenes	H ₂ (extracted on the Pd–Ru membrane)	H ₂ (in the product mixture at the outlet of reactor)	CH ₄	C ₂ H ₆	C ₂ H ₄	C ₃ H ₈	C ₄ H ₁₀	1,3-C ₄ H ₆
Granulated/contactor	46	35.9	0	23.6	5.6	0	3.0	0	0.1	2.8
Granulated/extractor	58	28.0	4.2	22.6	9.8	0	7.0	0.1	0.1	5.1
Integral/contactor	53	30.4	0	20.6	4.3	0.3	1.4	2.4	0.1	12.3
Integral/extractor	65	23.0	3.7	19.3	5.4	0.4	1.8	3.0	0.1	15.5

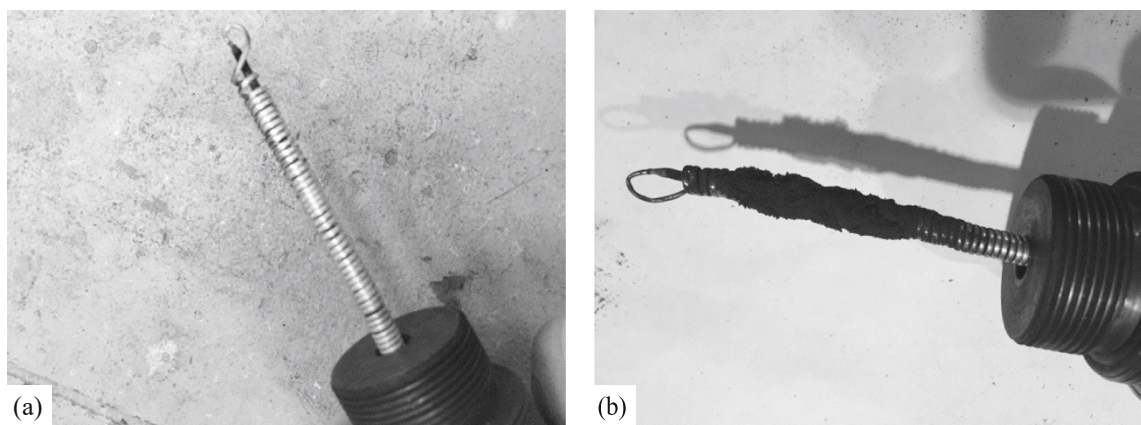


Fig. 4. Hydrogen-selective palladium-containing membrane after the dehydrogenation of the butene fraction (a) using integral $[\text{Fe,Cr}]/\gamma\text{-Al}_2\text{O}_3(\text{K,Ce})/\alpha\text{-Al}_2\text{O}_3$ converter and (b) on a granular converter of the same composition.

3. STUDIES OF THE SURFACE OF THE CATALYTIC CONVERTER

A TG analysis revealed insignificant carbonization of the spent integral $[\text{Fe,Cr}]/\gamma\text{-Al}_2\text{O}_3(\text{K,Ce})/\alpha\text{-Al}_2\text{O}_3$ converter in the air flow (Fig. 5).

The thermogravimetric data indicate that the degree of sample carbonization after 20 h was only 0.005 wt %. The oxidative regeneration was performed at 450–600 °C.

The dehydrogenation of the butene fraction into 1,3-butadiene for 20 h did not lead to a noticeable decrease in the catalytic activity of the system. This is an important advantage of the system over the industrial catalyst for dehydrogenation of the butane–butene fraction, which is generally regenerated every 8–15 min [28].

Therefore, we can conclude that the developed $[\text{Fe,Cr}]/\gamma\text{-Al}_2\text{O}_3(\text{K,Ce})/\alpha\text{-Al}_2\text{O}_3$ integral converters are stable against carbonization during dehydrogenation of the butene fraction to 1,3-butadiene, which makes them promising for practical applications. This is in good agreement with the results of previous studies that showed that the carbon dioxide reforming of methane was promoted in open catalytic channels of a porous converter and had significantly higher resistance to carbonization compared to the process in a conventional flow reactor with a loaded granular catalyst bed [19–21, 29].

A SEM-EDX analysis allowed us to evaluate the size factor and the distribution of active components on the surface of the $[\text{Fe,Cr}]/\gamma\text{-Al}_2\text{O}_3(\text{K,Ce})/\alpha\text{-Al}_2\text{O}_3$ converter (Fig. 6a). The distribution of the K, Ce, Fe, and Cr components on the support surface is quite uniform (Figs. 6b–6f). The particle size does not exceed 6 nm. The carbon content in the spent sample is low, indicating slight coking of the catalyst during the dehydrogenation of the butene fraction. The carbon distribution data presented in Fig. 6b refer to the carbon on the organic-based fixing glue required for fixing the sample on the stage of the electron microscope.

The active components of the $[\text{Fe,Cr}]/\gamma\text{-Al}_2\text{O}_3(\text{K,Ce})/\alpha\text{-Al}_2\text{O}_3$ converter were visualized and spectrally identified and their particle size on the support surface was determined before and after the catalytic tests using TEM-EDX analysis.

On the initial catalyst, the iron- and chromium- containing components were uniformly distributed over the surface of the $\alpha\text{-Al}_2\text{O}_3$ support, but some regions contained distinct clusters with sizes of up to 100–150 nm containing highly dispersed particles of metal-containing active components (Figs. 7a–7c).

In the spent converter, there were no visible changes in the particle size of the deposited Fe and Cr components. There was no surface carbonization, which indicates high resistance of the sample to coke formation during the dehydrogenation of butenes.

Figure 8 shows the Fe2p and Cr2p XPS spectra of the initial $[\text{Fe,Cr}]/\gamma\text{-Al}_2\text{O}_3(\text{K,Ce})/\alpha\text{-Al}_2\text{O}_3$ converter. Only some part of the 2p_{3/2} spectrum was processed for both metals after

subtracting the background component by the Shirley method. The spectra were identified using the database [30].

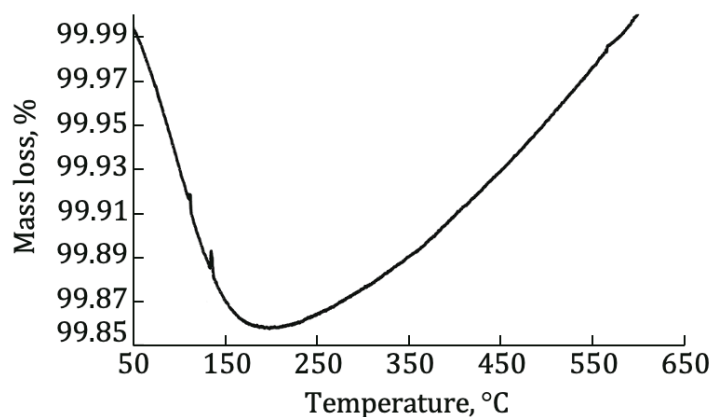


Fig. 5. TG analysis in the air flow of the [Fe,Cr]/ γ -Al₂O₃(K,Ce)/ α -Al₂O₃ converter. The low peaks in the temperature range 100–150 °C correspond to water desorption.

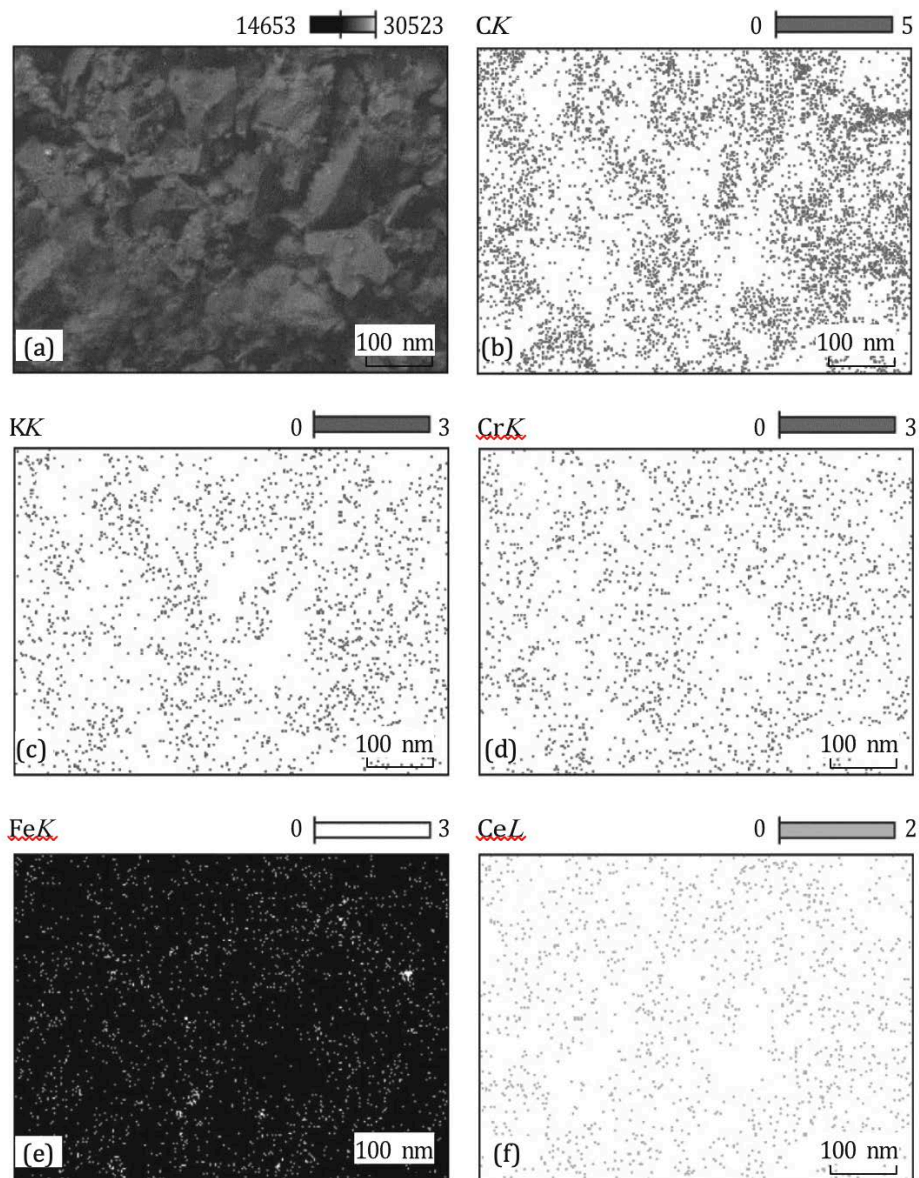


Fig. 6. Images of the (a) scanned surface of the spent [Fe,Cr]/ γ -Al₂O₃(K,Ce)/ α -Al₂O₃ converter and (b–f) distribution of active components: (b) C, (c) K, (d) Cr, (e) Fe, and (f) Ce on it according to SEM-EDX analysis data.

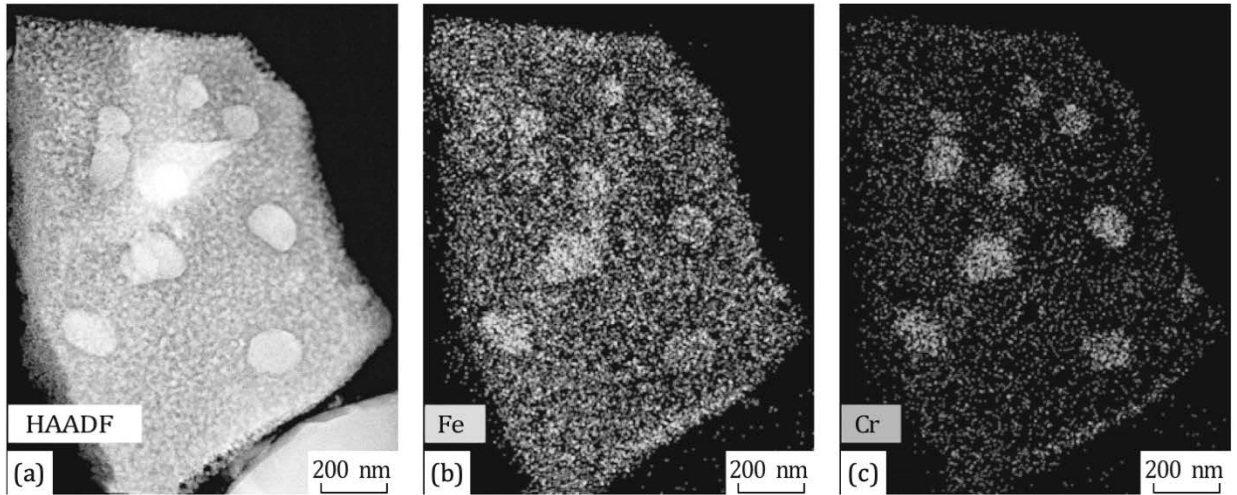


Fig. 7. Images of the (a) scanned surface of the initial [Fe,Cr]/ γ -Al₂O₃(K,Ce)/ α -Al₂O₃ converter and (b), (c) distribution of (b) Fe and (c) Cr particles and agglomerates on it.

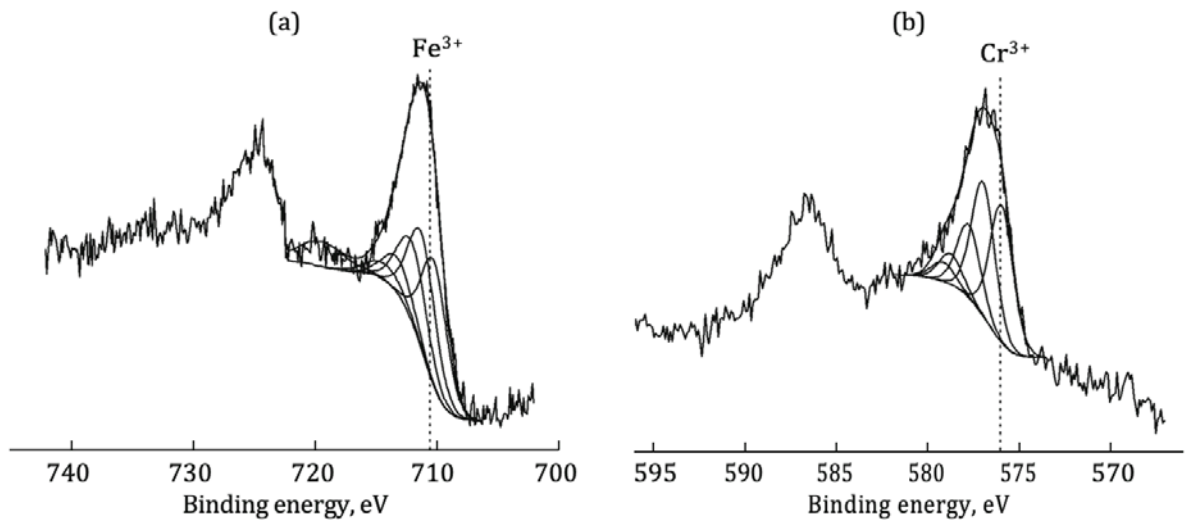


Fig. 8. (a) Fe2p and (b) Cr2p XPS spectra of the initial [Fe,Cr]/ γ -Al₂O₃(K,Ce)/ α -Al₂O₃ converter.

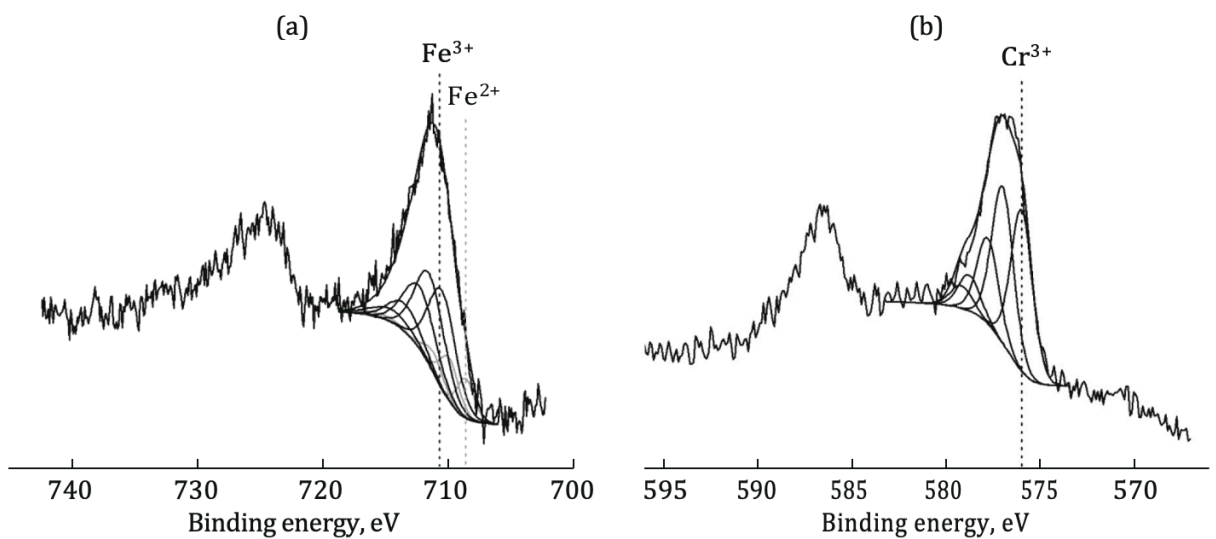


Fig. 9. (a) Fe2p and (b) Cr2p XPS spectra of the spent [Fe,Cr]/ γ -Al₂O₃(K,Ce)/ α -Al₂O₃ converter.

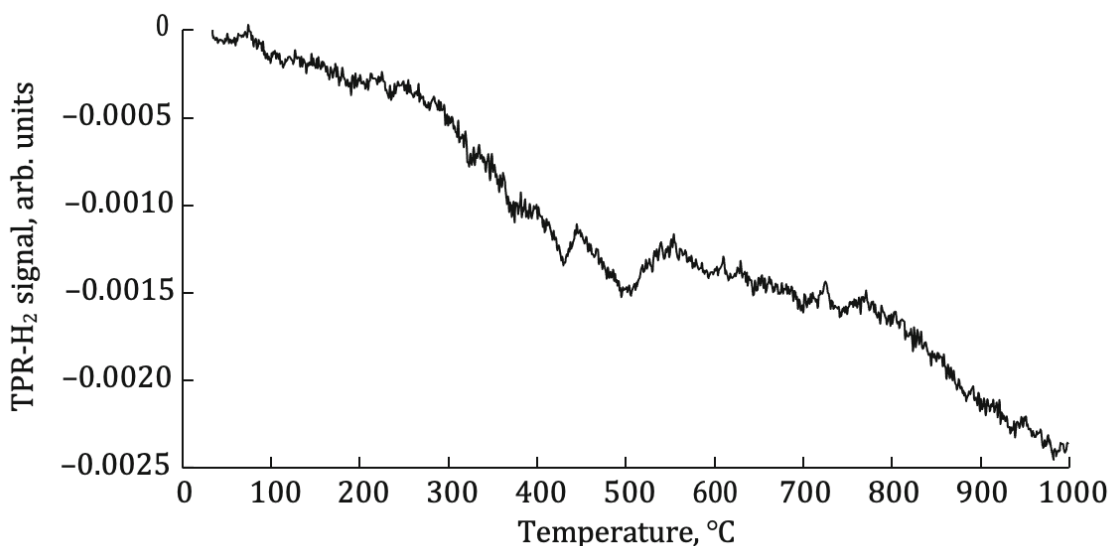


Fig. 10. TPR-H₂ profile of the initial [Fe,Cr]/ γ -Al₂O₃(K,Ce)/ α -Al₂O₃ converter.

It was found that, in accordance with the results of the decomposition of the Fe2p spectrum, iron is in the oxidation state +3; the binding energy of the main peak is 710.2 eV, and that of the satellite peak is 9.3 eV higher.

The Cr2p spectrum contains a main peak with a binding energy of 576.0 eV and four multiplet peaks. The presence of these peaks suggests that the initial converter contained chromium oxide Cr₂O₃ particles in addition to iron oxides.

The data obtained in the decomposition of the Fe2p spectrum (Fig. 9a) suggest the presence of reduced forms of iron in the converter.

The XPS studies of the spent converter indicate that in addition to Fe³⁺, the Fe²⁺ component is present, whose peak is localized in the energy region of 708.5 eV. It was found that the Fe²⁺ content was ~25% of the total amount of iron in the sample. This suggests partial reduction of iron with hydrogen during the catalytic process.

There were no changes in the Cr2p spectrum after catalysis. This means that chromium does not change its oxidation state during the process and is in the Cr+3 state, as it was in the initial sample (Fig. 9b).

The data of programmed thermal reduction with hydrogen showed the presence of a small peak (0.00184 mmol/g) in the temperature range 494.5 °C of the initial [Fe,Cr]/ γ -Al₂O₃(K,Ce)/ α -Al₂O₃ converter. At these temperatures, Fe(III) oxide is partially reduced to nonstoichiometric magnetite (Fig. 10):



The obtained result correlates well with the XPS data, indicating that during dehydrogenation, the spent sample is reduced with liberated hydrogen to nonstoichiometric magnetite, in which some part of Fe⁺³ ions are reduced to Fe⁺².

CONCLUSIONS

The synthesized catalytic [Fe,Cr]/ γ -Al₂O₃(K,Ce)/ α -Al₂O₃ converter containing open channels with sizes of 1–3 μm is characterized by a highly porous structure and can be regarded as an assembly of microreactors. The diffusion of reagent vapors in a limited pore volume apparently leads to increased transverse diffusion and increased probability of contact of the gaseous substrates with the active surface [31]. This explains the intensification of the catalytic reactions, in particular, dehydrogenation, and an increase in the resistance to coke formation.

ACKNOWLEDGMENTS

We are grateful to D.O. Antonov for his help in performing catalytic experiments, and to Benjamin Katryniok, Joelle Thuriot, and Olivier Gardoll for help with SEM-EDX, XRD, and TG analyses.

A.S. Fedotov thanks the Embassy of France in Moscow for awarding him the “Mechnikov scholarship-2018: Scientific visits,” which made it possible to perform a wide range of structural analyses at the Catalysis and Solid State Chemistry Laboratory of the Lille University.

We also thank Chevreul Institute (FR 2638); Ministry of Higher Education, Research, and Innovation; Hauts-de-France region; National Center for Scientific Research; European Regional Development Fund; École centrale de Lille; and Central Initiative Fund for financial support.

FUNDING

This study was supported by the Russian Science Foundation (grant no. 17-13-01270).

REFERENCES

1. Lebedev, S.V., Zh. Ross. Khim. Obshch., 1909, vol. 41, p. 42.
2. White, W.C., *Chem.–Biol. Interact.*, 2007, vol. 166, nos. 1–3, p. 10
3. Doelle, H.W., Rokem, J.S., and Berovic, M., *Biotechnology, V. IV: Fundamentals in Biotechnology*, Oxford: Eolss, 2009.
4. Ochoa, J.V., Bandinelli, C., Vozniuk, O., Chiericato, A., Malmusi, A., Recchi, C., and Cavani, F., *Green Chem.*, 2016, vol. 18, no. 6, p. 1653.
5. Farzad, S., Mandegari, M.A., and Görgens, J.F., *Bioresour. Technol.*, 2017, vol. 239, p. 37.
6. IHS Markit, Chemical Economics Handbook, Globalbutadiene production overview. <https://ihsmarkit.com/products/butadiene-chemical-economics-handbook.html>. Accessed July 25, 2019.
7. Makshina, E.V., Dusselier, M., Janssens, W., Degève, J., Jacobs, P.A., and Sels, B.F., *Chem. Soc. Rev.*, 2014, vol. 43, no. 22, p. 7917.
8. Arpe, H-J. and Hawkins, S. *Industrial Organic Chemistry*, New York: Wiley, 2010, 5th ed., p. 525.
9. Kondakov, I.L., Sinteticheskii kauchuk ego gomologi i analogi: Tip. Mattisena (Synthetic Rubber its Homologies and Analogies. Matissen Type), 1912, p. 151.
10. Zhang, J., Wang, S., and Wang, Y. *Advances in Bioenergy*, Ch. 1: Biobutanol Production from Renewable Resources Recent Advances, Elsevier: Netherlands, 2016, vol. 1, p. 1.
11. Doelle, H.W., Rokem, J.S., and Berovic, M., *Biotechnology, V. VI: Fundamentals in Biotechnology*, Oxford: Eolss, 2009.
12. Silvester, L., Lamonier, J.F., Lamonier, C., Capron, M., Vannier, R.N., Mamede, A.S., and Dumeignil, F., *ChemCatChem*, 2017, vol. 9, no. 12, p. 2250.
13. Tsodikov, M.V., Yandieva, F.A., Kugel, V.Y., Chistyakov, A.V., Gekhman, A.E., and Moiseev, I.I., *Catal. Lett.*, 2008, vol. 121, nos. 3–4, p. 199.
14. Tsodikov, M.V., Chistyakov, A.V., Nikolaev, S.A., Kriventsov, V.V., Gekhman, A.E., and Moiseev, I.I., *Chemistry of Biomass. Biofuels and Bioplastics: Scientific Word*, 2017, p. 223.
15. Research and Markets, Global Bio-Butanol Market. Segmented by Application and Geography 2017–2022. <https://www.researchandmarkets.com/reports/4390693/global-bio-butanol->

market-segmented-by. Cited July 25, 2019.

16. Biomass Magazine, Minnesota n-butanol plant comes online. <http://biomassmagazine.com/articles/14006/minnesota-butanol-plant-comes-online>. Accessed July 25, 2019.
17. Stabnikov, V.N., *Peregonka i rektifikatsiya etilovogo spir-ta* (Distillation and Rectification of Ethyl Alcohol), Moscow: Pishchevaya Promyshlennost', 1969, 2nd ed., p. 456.
18. Chistyakov, A.V., Zharova, P.A., Tsodikov, M.V., Niko-laev, S.A., Krotova, I.N., and Ezzhelenko, D.I., *Kinet. Catal.*, 2016, vol. 57, no. 6, p. 803.
19. Fedotov, A.S., Antonov, D.O., Uvarov, V.I., and Tso-dikov, M.V., *Int. J. Hydrogen Energy*, 2018, vol. 43, no. 14, p. 7046.
20. Tsodikov, M.V., Fedotov, A.S., Antonov, D.O., Uvarov, V.I., Bychkov, V.Y., and Luck, F.C., *Int. J. Hy-drogen Energy*, 2016, vol. 41, no. 4, p. 2424.
21. Fedotov, A.S., Antonov, D.O., Bukhtenko, O.V., Uvarov, V.I., Kriventsov, V.V., and Tsodikov, M.V., *Int. J. Hydrogen Energy*, 2017, vol. 42, no. 38, p. 24131.
22. Kantaev, A.S. and Brus, I.D., *Opredelenie razmera por fil'truyushchego elementa* (Determination of Pore Size of Filtering Element), Tomsk: Tomsk Polytechnic Uni-versity, 2014, p. 16.
23. Gucci, L. and Erdöhelyi, A., *Catalysis for Alternative Energy Generation*, Berlin: Springer, 2012, p. 538.
24. Khan, Y., Marin, M., Karinen, R., Lehtonen, J., and Kanervo, J., *Chem. Eng. Sci.*, 2015, vol. 137, p. 740.
25. Grub, J. and Löser, E., Butadiene, in *Ullmann's Ency-clopedia of Industrial Chemistry*, Weinheim: Wiley, 2012.
26. Berteau, P., Ruwet, M., and Delmon, B., *Bull. Des So-ciétés Chim. Belges*, 1985, vol. 94, nos. 11–12, p. 859.
27. Phung, T.K., Lagazzo, A., Rivero Crespo, M.Á., Sán-chez Escribano, V., and Busca, G., *J. Catal.*, 2014, vol. 311, p. 102.
28. Tyuryaev, I.Ya., *Usp. Khim.*, 1966, vol. 35, no. 1, p. 121.
29. Fedotov, A.S., Antonov, D.O., Uvarov, V.I., Tso-dikov, M.V., and Khadzhiev, S.N., *Pet. Chem.*, 2018, vol. 58, no. 1, p. 62.
30. Biesinger, M.C., Payne, B.P., Grosvenor, A.P., Lau, L.W., Gerson, A. R., and Smart, R.S.C., *Appl. Surf. Sci.*, 2011, vol. 257, no. 7, p. 2717.
31. Teplyakov, V.V. and Tsodikov, M.V., *Porous Inorganic Membrane Reactors. In Simulation of Membrane Reac-tors*, Ed. A. Basile and F. Gallucci, New York: Nova Science, 2009, p. 123.